RSC Advances

PAPER

View Article Online
View Journal | View Issue

Cite this: *RSC Adv.*, 2026, **16**, 18757

Synthesis and functionalization of a Chitosan-PEI-Metallothionein biopolymer with enhanced mechanical and adsorptive properties for heavy metal removal

Nafiseh Sheykhan,[a] Majid Ghashang *[a] and Agata Szuławska-Mroczek[b]

A novel biofunctionalized polymeric adsorbent, Chitosan-Polyethyleneimine-Metallothionein-like Proteins (Chitosan-PEI-MTLPs), was synthesized through a controlled multi-step grafting and immobilization strategy. Mechanical analysis revealed a substantial enhancement in mechanical integrity following PEI grafting and MTLP conjugation, with the flexural strength (FS) increasing from 25.48 MPa (chitosan) to 68.75 MPa (Chitosan-PEI-MTLPs), and compressive strength (CS) rising from 51.25 MPa to 129.35 MPa. Water absorption increased from 19.9% to 32%, indicating improved hydrophilicity and porosity. The synthesized biocomposite demonstrated exceptional adsorption performance for Cd(II), Ni(II), and Pb(II) ions, achieving maximum removal efficiencies of 93%, 89%, and 95%, respectively, at pH 6.5 and 45 °C. Kinetic studies confirmed a pseudo-first-order model, suggesting a predominantly physical adsorption process. Reusability tests demonstrated excellent regeneration capability, with 89–91% capacity retention after eleven cycles. These findings establish the Chitosan-PEI-MTLPs polymer as a highly stable, reusable, and biocompatible adsorbent with potential for selective heavy metal remediation in aqueous systems.

Received 22nd November 2025
Accepted 26th February 2026

DOI: 10.1039/d5ra09022a

rsc.li/rsc-advances

1. Introduction

The contamination of aquatic ecosystems by heavy metals, particularly lead (Pb) and cadmium (Cd), poses significant environmental and public health challenges due to their toxicity, persistence, and bio-accumulative nature. These metals can cause severe health issues, including neurological disorders and kidney damage, even at low concentrations.[1,2] In response to the persistent challenges posed by heavy metal contamination in aqueous environments, a variety of remediation strategies have been developed, including membrane filtration, ion exchange, electrochemical treatment, chemical precipitation, and adsorption.[3] While many of these techniques offer high removal efficiencies, they are often associated with significant drawbacks such as high operational costs, sludge generation, limited selectivity, and sensitivity to pH fluctuations. Among them, adsorption has emerged as one of the most promising methods due to its simplicity, low energy requirements, high efficiency even at low contaminant concentrations, and adaptability to various operational conditions.[4–6]

Particularly, the use of bio-based polymeric adsorbents has gained significant momentum in recent years. Natural polymers such as cellulose, chitosan, and their chemically modified derivatives are considered excellent candidates owing to their abundance, renewability, environmental friendliness, and the presence of abundant hydroxyl, amine, and carboxyl functional groups, which facilitate strong interactions with metal ions through complexation, ion exchange, and electrostatic attraction mechanisms. Moreover, the structural versatility of these biopolymers allows for various modifications such as grafting, crosslinking, magnetization, and functionalization, further enhancing their physicochemical stability, mechanical strength, and adsorption capacity. These advancements have propelled the development of next-generation adsorbents capable of efficient and selective removal of toxic metals such as Pb(II), Cd(II), Hg(II), and Cr(VI) from complex wastewater matrices.[7–26]

Among various biomolecules with metal-binding capabilities, metallothioneins (MTs)-low molecular weight, cysteine-rich proteins naturally present in the tissues of many vertebrates have emerged as potent candidates for the selective sequestration of heavy metals. These proteins exhibit an exceptional affinity for divalent metal ions such as Cd(II) and Pb(II) due to abundant thiol (−SH) groups from cysteine residues, which enable the formation of stable metal-thiolate clusters through coordination bonding. As such, MTs play

[a]*Department of Chemistry, Na.C., Islamic Azad University, Najafabad, Iran. E-mail: ghashangmajid@gmail.com; Ghashangmajid@iau.ac.ir*
[b]*Department of Biomedical Chemistry, Faculty of Health Sciences, Medical University of Lodz, 92-215, Lodz, Poland*

a crucial role in metal homeostasis and detoxification in biological systems and hold significant promise as bio-adsorbents in engineered water treatment platforms.[27–30]

However, the practical application of free metallothioneins is hindered by their limited mechanical strength, susceptibility to denaturation, and difficulty in recovery and reuse. To overcome these limitations, immobilization of MTs onto stable solid supports or within polymeric matrices has been explored. In particular, chitosan and polyethylene imine (PEI) have garnered attention due to their complementary physicochemical properties. Chitosan have limited hydrophilicity due to strong intermolecular hydrogen bonding and partial crystallinity, which restrict its solubility and accessibility of active sites and commonly used in separation technologies, while PEI is a highly branched polymer rich in primary, secondary, and tertiary amine groups, offering multiple coordination sites for heavy metal ions and facilitating covalent or electrostatic interactions with proteins.

The crosslinking of MTs with a Chitosan-PEI matrix can effectively enhance the mechanical integrity, thermal stability, and reusability of the protein-based adsorbent while preserving its high metal-binding functionality. Moreover, such crosslinked systems can provide synergistic adsorption sites combining thiol and amine functionalities, which improve selectivity and uptake performance in the presence of competitive ions. Despite their potential, studies on the integration of naturally extracted MTs into polymeric networks for environmental remediation are still limited.

Therefore, the aim of the present work is: to extract and purify metallothionein proteins from sheep liver and kidney tissues, to incorporate and stabilize these proteins within a chitosan-PEI crosslinked polymeric network, and to evaluate the performance of the resulting hybrid adsorbent in the removal of hazardous heavy metal ions, specifically Pb(II), Ni(II), and Cd(II) ions from aqueous solutions under environmentally relevant conditions.

2. Experimental

2.1. Reagents and instrumentation

All reagents used in this study were of analytical grade and employed without further purification. Chitosan (degree of deacetylation ≥95%, medium molecular weight), polyethyleneimine (PEI, branched, Mw = 25 000 g mol^{-1}), chloroacetyl chloride (≥99%), *N*,*N*-dimethylformamide (DMF, anhydrous, 99.8%), diethyl ether (≥99%), acetone (≥99.5%), Tris(hydroxymethyl)aminomethane (Tris–HCl), phenylmethylsulfonyl fluoride (PMSF, ≥98%), and dithiothreitol (DTT, ≥99%) were purchased from Merck (Darmstadt, Germany). Cadmium nitrate hexahydrate ($Cd(NO_3)_2 \cdot 6H_2O$, ≥99.5%), lead nitrate hexahydrate ($Pb(NO_3)_2 \cdot 6H_2O$, ≥99%), and nickel nitrate hexahydrate ($Ni(NO_3)_2 \cdot 6H_2O$, ≥99%) were obtained from Sigma-Aldrich (St. Louis, MO, USA).

The instruments employed were of high precision and regularly calibrated before use. Heavy metal ion concentrations were determined using an atomic absorption spectrophotometer (Shimadzu, AA-6880, Japan). Thermal behavior was analyzed *via* thermogravimetric and differential thermogravimetric (TGA-DTG) measurements using a Shimadzu TGA-DTG-60H instrument under a nitrogen atmosphere. Fourier-transform infrared (FT-IR) spectra were recorded using a Bruker spectrophotometer on KBr pellets in the range 400–4000 cm^{-1}. Surface morphology and elemental composition were examined by field emission scanning electron microscopy (FE-SEM) coupled with energy-dispersive X-ray spectroscopy (EDX) using a JEOL JSM-IT100 microscope. All experiments were performed in triplicate to ensure reproducibility and precision.

2.2. Extraction procedure for metallothionein-like proteins (MTLPs) from sheep tissues

Metallothionein-like proteins (MTLPs) were extracted from the liver tissue of *Lori-Bakhtiari* sheep using a modified heat-stable protein isolation protocol to ensure purity and preservation of thiol functionality. Fresh liver samples were obtained from local certified slaughterhouses under sterile conditions and immediately transported on ice to the laboratory. Samples were rinsed with cold isotonic saline and homogenized (1 : 5 w/v) in ice-cold 20 mM Tris–HCl buffer (pH 7.4) containing 0.1 mM PMSF and 1 mM DTT to inhibit proteolysis and maintain reduced thiol groups. The homogenate was heated at 80 °C for 10 min to denature heat-labile proteins, followed by rapid cooling on ice and centrifugation at 15 000 × *g* for 30 min at 4 °C. The supernatant, containing heat-stable MTLPs, was subjected to ammonium sulfate precipitation (80% saturation) and centrifuged again under the same conditions. The precipitate was dissolved in Tris-HCl buffer and dialyzed overnight (10 kDa MWCO) against the same buffer to remove residual salts. The purity and integrity of the isolated MTLPs were confirmed by UV absorbance at 254 nm, Ellman's assay for sulfhydryl quantification, and SDS-PAGE, which revealed a distinct band at approximately 6–7 kDa consistent with the molecular mass of metallothioneins.

2.3. Preparation of Chitosan-PEI-MTLPs polymeric system

The Chitosan-PEI-MTLPs composite was synthesized *via* a controlled, multi-step functionalization strategy (Scheme 1). Chitosan (1 g) was first dissolved in anhydrous DMF and reacted with chloroacetyl chloride (5 mL) under a nitrogen atmosphere at 0 °C for 30 min, followed by reflux at 110 °C for 3 h. The reaction mixture was cooled, and the product was precipitated in cold diethyl ether, filtered, washed thoroughly with acetone, and vacuum-dried at 40 °C. The resulting chloroacetylated chitosan was then reacted with branched PEI (M_w = 25 000 g mol^{-1}) in DMF under reflux at 110 °C for 10 h to produce the crosslinked Chitosan-PEI polymer. The product was precipitated in cold acetone, washed, and vacuum-dried. For further activation, the polymer was re-treated with chloroacetyl chloride under identical conditions for 10 h. Protein immobilization was achieved by dispersing the activated Chitosan-PEI in phosphate-buffered saline (PBS, pH 7.4) and adding the MTLPs solution dropwise under gentle nitrogen flow to prevent thiol oxidation. The reaction was stirred at 37 °C for 10 h, followed by dialysis (MWCO = 10 kDa) against deionized water for 48 h to

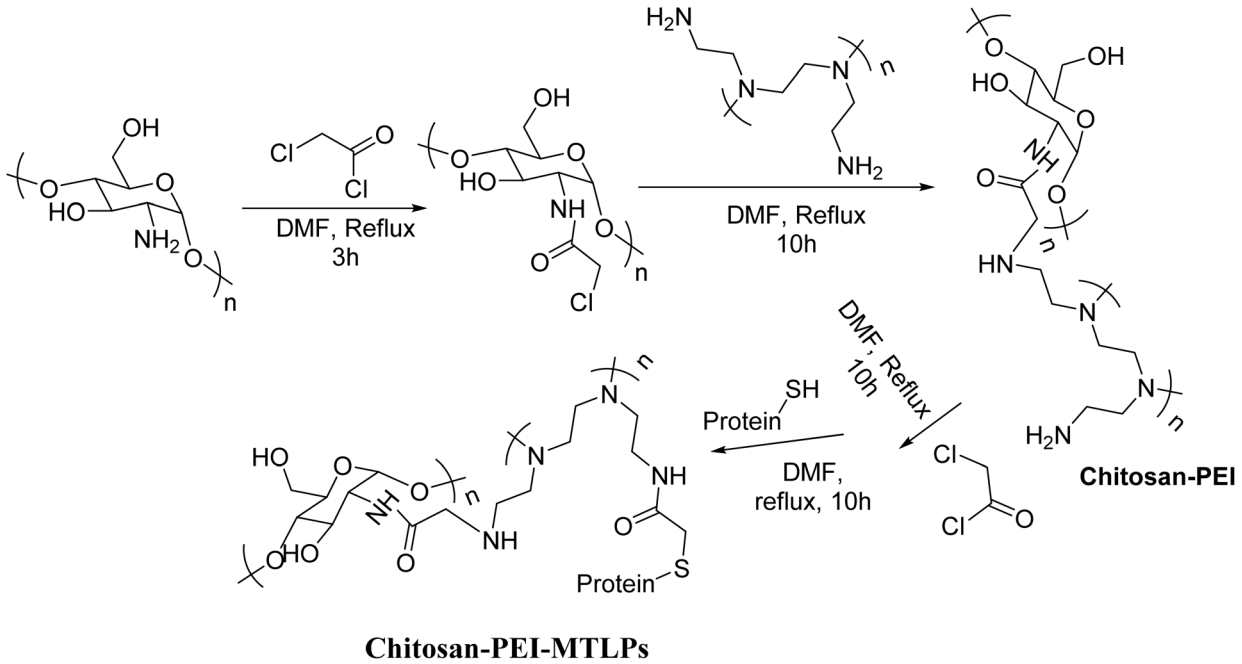

Scheme 1 Schematic preparation of the chitosan-PEI-MTLPs polymeric system.

remove unbound species. The purified Chitosan-PEI-MTLPs polymer was lyophilized to yield a pale yellow solid. The final product exhibited high purity, confirmed by FT-IR, elemental analysis, and the absence of unreacted species in the filtrate.

2.4 Adsorption experiments

Stock solutions of heavy metal ions were prepared by dissolving precise amounts of cadmium nitrate hexahydrate ($Cd(NO_3)_2 \cdot 6H_2O$) for Cd^{2+} and lead nitrate hexahydrate ($Pb(NO_3)_2 \cdot 6H_2O$) for Pb(II) ions in deionized water to obtain concentrations of 200, 400, 600, 800, and 1000 mg L^{-1}. To investigate the effect of pH on the adsorption process, the pH of these solutions was adjusted within the range of 4 to 8 using diluted solutions of sodium hydroxide (1 M NaOH) and hydrochloric acid (1 M HCl). For the adsorption experiments, 0.06 g of the Chitosan-PEI-MTLPs polymer (1.2g L^{-1}) was added to 50 mL of heavy metal ion solution with an initial concentration of 800 mg L^{-1} in a 250 mL Erlenmeyer flask. The mixture was stirred at room temperature for 120 minutes to reach adsorption equilibrium, after which it was filtered and the remaining metal ion concentration in the filtrate was analyzed using atomic absorption spectroscopy (AAS). The study systematically examined the influence of key parameters on the adsorption process, including pH (4–8), initial metal ion concentration (200–1000 mg L^{-1}), adsorbent dosage (0.3–1.5 g L^{-1}), and temperature (25–65 °C). The adsorption performance was evaluated by calculating the equilibrium adsorption capacity (q_e) using standard adsorption equations.

$$q_e = \frac{C_0 - C_e V}{m},\ q_e = \frac{C_0 - C_t V}{m}$$

where C_0 is the initial concentration (mg L^{-1}), C_e is the equilibrium concentration (mg L^{-1}), m is the mass of the adsorbent (g), V is the solution volume (L), and q_t represents the adsorption capacity at time t.

For the recovery process, the used samples were washed three times with HCl solution (0.01 M). Subsequently, the material was treated with a salt solution (NaCl, 5%) and stirred at room temperature for 30 min. After stirring, the suspension was centrifuged and the supernatant was decanted. In the next step, an EDTA solution (1 M) was applied to release the adsorbed heavy metals, and the mixture was stirred for an additional 30 min. Finally, the sample was separated and washed three times with deionized water to remove residual reagents before reuse.

2.5. Evaluation of mechanical characteristics

Once synthesized, the materials were placed into aluminum alloy molds, followed by vacuum degassing to eliminate trapped air. Initial polymerization was carried out using an LED curing device for 60 seconds. Test specimens were produced with dimensions of 40 mm (length), 15 mm (width), and 2 mm (thickness). To ensure full crosslinking, the samples were subsequently heat-treated at 120 °C for a duration of 2 hours. Mechanical testing including measurements of flexural strength (FS), flexural modulus (FM), and compressive strength (CS) was conducted using an Instron 6025 universal testing system, operating at a speed of 10 mm min^{-1} under a maximum load of 100 kN. All mechanical evaluations adhered to the ISO 10477 : 1992 standard. Each test was repeated three times to confirm consistency and minimize random errors.[6]

2.6. Assessment of water uptake

Water absorption performance was tested using samples sized 10 × 10 × 3 mm^3. Before testing, all specimens were dried to a constant mass and weighed using a precision digital scale (Denver, model AA-200, USA). The dried samples were immersed in 30 mL of distilled water (neutral pH 7), kept at 25 ° C in sealed vessels. At regular intervals, the samples were taken out, gently blotted to remove surface moisture, reweighed, and returned to the containers. This process continued until the recorded weights stabilized, indicating saturation. Each experiment was carried out in triplicate to enhance reliability.

The extent of water absorption was calculated using the following formula:

Eqn (1):

$$M(\%) = \frac{W - W}{W_0} \times 100 \quad (1)$$

where W_0 is the sample's initial dry mass, and W_t is the mass at a given time t.[6]

3. Results and discussion

3.1. Schematic preparation and characterization of chitosan-PEI-MTLPs polymer

The chitosan-PEI-MTLPs polymeric system was synthesized through a controlled multi-step functionalization strategy designed to produce an amine-rich scaffold for efficient protein immobilization (Scheme 1). Initially, chitosan was reacted with chloroacetyl chloride in anhydrous DMF under nitrogen to introduce reactive acyl chloride groups. Subsequently, branched PEI was grafted onto the modified chitosan *via* nucleophilic substitution, yielding a highly amine-functionalized Chitosan-PEI framework. A second treatment with chloroacetyl chloride introduced additional electrophilic sites, enabling covalent attachment of thiol-containing metallothionein-like proteins (MTLPs). Finally, MTLPs were immobilized onto the activated polymer, forming the Chitosan-PEI-MTLPs bioconjugate.

Elemental (CHNS) analysis confirmed the stepwise modification of chitosan and successful incorporation of MTLPs (Table 1). The attachment of chloroacetyl groups slightly increased carbon and nitrogen contents to 37.59% and 5.48%, respectively. PEI grafting caused a marked rise in carbon (47.02%) and nitrogen (17.98%) contents, consistent with PEI's high amine density. In the final Chitosan-PEI-MTLPs composite, slight reductions in carbon (45.03%), hydrogen (7.98%), and nitrogen (17.02%) contents were observed due to partial surface coverage by MTLPs, while the emergence of sulfur (8.97%) confirmed their successful incorporation. These results collectively demonstrate effective functionalization, PEI grafting, and sulfur-bearing MTLP immobilization within the polymer matrix.

FT-IR analysis further validated these modifications (Fig. 1). The spectrum of chitosan–NH–CO–CH_2–Cl displayed characteristic peaks at 3300–3800 cm^{-1} (NH/OH stretching), 2850–2950 cm^{-1} (C–H, sp^3), 1650–1700 cm^{-1} (amide C═O), and 700–850 cm^{-1} (C–Cl stretching). After PEI grafting, the disappearance of the C–Cl band and enhanced NH/OH stretching indicated successful conjugation. The Chitosan-PEI-MTLPs spectrum showed a new band near 2500–2600 cm^{-1}, corresponding to S–H stretching, confirming the presence of thiol groups from MTLPs. The emergence of a double N–H stretching band, arises from the simultaneous presence of amide groups and primary/secondary amines introduced by PEI modification. These results corroborate the sequential modification of chitosan, PEI integration, and MTLP attachment, confirming the structural evolution of the composite (Fig. 1).

Mechanical testing (Fig. 2) revealed progressive enhancement in flexural modulus (FM), diametral tensile strength (DTS), compressive strength (CS), and flexural strength (FS) following PEI grafting and MTLP incorporation. Pure chitosan exhibited limited mechanical performance (FM: 2.01 GPa; DTS:

Table 1 CHNS elemental analysis of Chitosan–NH–CO–CH_2–Cl, chitosan-PEI, and chitosan-PEI-MTLPs polymeric systems

Sample	% C	% H	% N	% S
Chitosan–NH–CO–CH_2–Cl	37.59	5.52	5.48	—
Chitosan-PEI	47.02	8.28	17.98	—
Chitosan-PEI-MTLPs	45.03	7.98	17.02	8.97

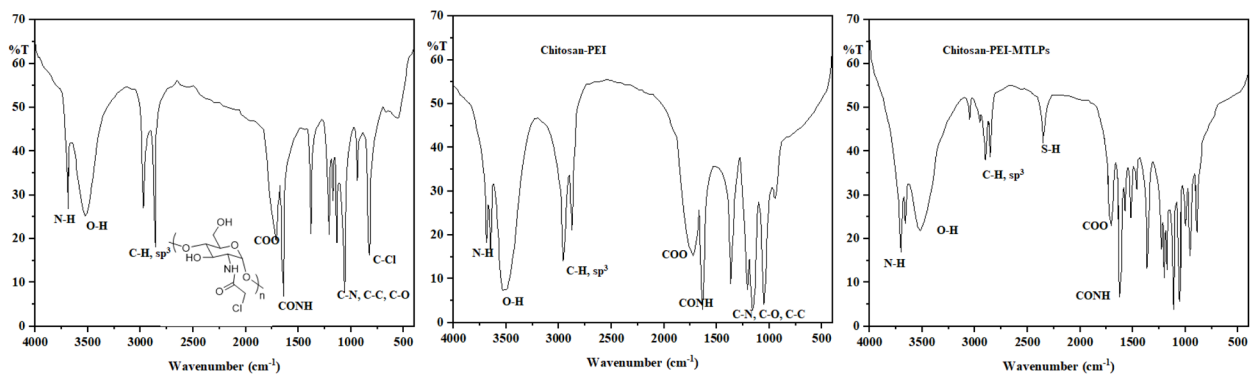

Fig. 1 FT-IR analysis of chitosan–NH–CO–CH_2–Cl, Chitosan-PEI, and chitosan-PEI-MTLPs polymeric systems.

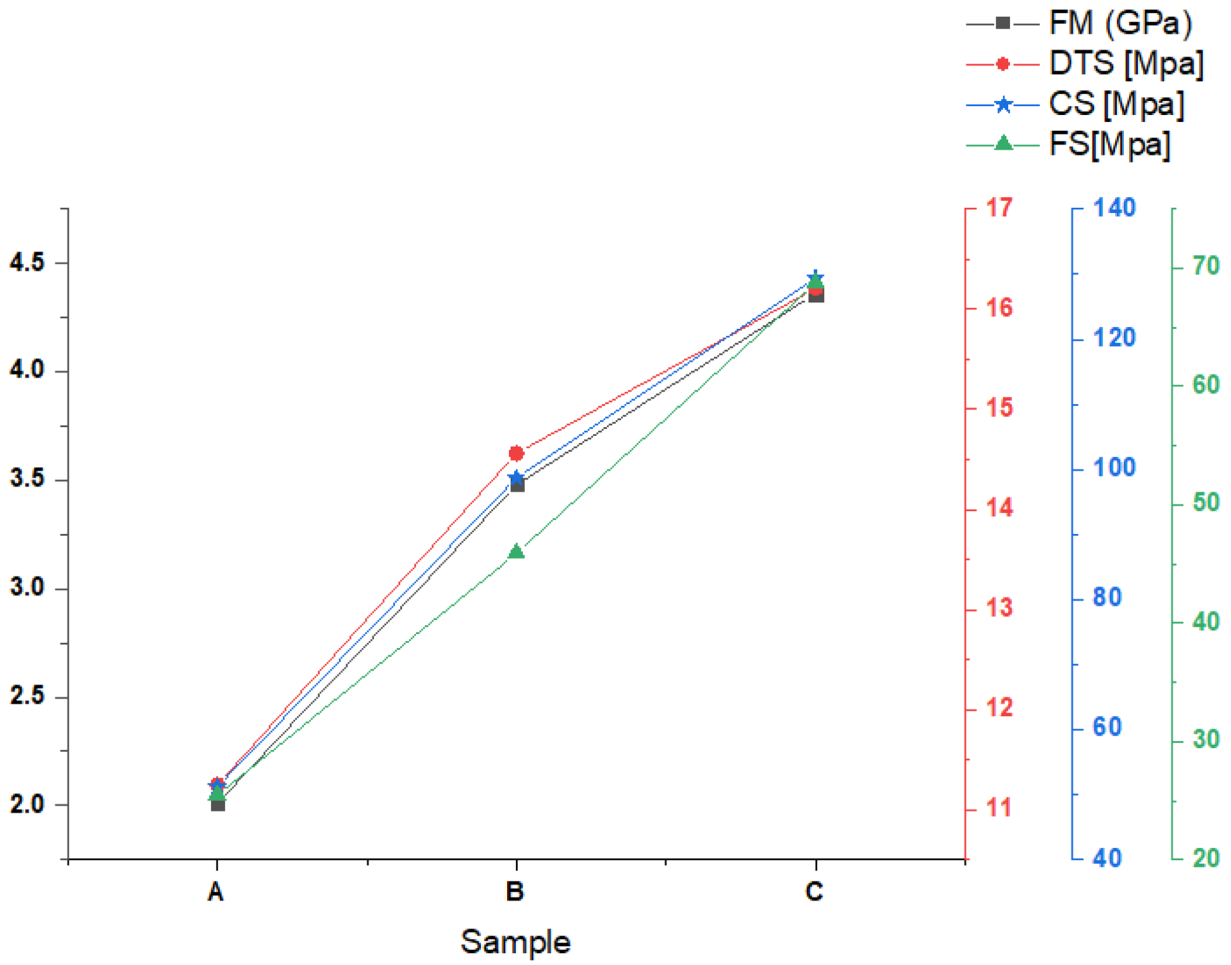

Fig. 2 Mechanical properties of chitosan (A), chitosan-PEI (B), and chitosan-PEI-MTLPs polymeric systems (C).

11.25 MPa; CS: 51.25 MPa; FS: 25.48 MPa), reflecting its inherent brittleness. PEI grafting significantly improved all parameters (FM: 3.48 GPa; DTS: 14.56 MPa; CS: 98.78 MPa; FS: 45.90 MPa), attributed to enhanced crosslinking and molecular entanglement within the amine-rich PEI network. The Chitosan-PEI-MTLPs composite showed the highest mechanical strength (FM: 4.36 GPa; DTS: 16.21 MPa; CS: 129.35 MPa; FS: 68.75 MPa), resulting from the rigid MTLP domains that restrict polymer chain motion and improve stress transfer through coordination with PEI functional groups.

Water uptake studies (Fig. 3) showed increasing hydrophilicity with each modification. Pure chitosan absorbed 19.9% water, while Chitosan-PEI and Chitosan-PEI-MTLPs absorbed 26.1% and 32%, respectively. The higher absorption reflects the abundance of amine and hydroxyl groups introduced by PEI and additional hydrophilic sites from MTLPs, which enhance water binding and porosity. The rapid initial uptake and plateau after 40 $h^{1/2}$ indicate efficient diffusion and stable water retention. These improvements demonstrate that sequential functionalization not only strengthens the polymer matrix but also enhances its hydrophilic behavior, making it suitable for applications in hydrogels, biomedical scaffolds, and sorbent materials.

3.2. Adsorption studies for Cd(II)/Ni(II)/pb(II) ions

The adsorption behavior of Cd(II), Ni(II), and Pb(II) ions on the Chitosan-PEI-MTLPs network showed a strong dependence on solution pH in the range of 4–8 (Fig. 4). At acidic conditions (pH = 4), relatively low adsorption capacities were observed, measuring 106 mg g^{-1} for Cd(II), 90.8 mg g^{-1} for Ni(II), and 121.4 mg g^{-1} for Pb(II). This diminished performance is primarily attributed to the high concentration of protons, which compete with metal ions for available binding sites. In addition, extensive protonation of amino, hydroxyl, and thiol groups within chitosan, PEI, and MTLPs reduces the availability of electron-donating sites necessary for effective metal coordination. As the pH increased, adsorption capacities improved substantially. Maximum adsorption was achieved at pH 6.5, with capacities of 620.1 mg g^{-1} for Cd(II), 593.36 mg g^{-1} for Ni(II), and 633.35 mg g^{-1} for Pb(II). Beyond pH 6.5, adsorption efficiency declined, mainly due to the formation of insoluble metal hydroxides ($Cd(OH)_2$, $Ni(OH)_2$, and $Pb(OH)_2$), which decreases the concentration of free metal ions available for sorption. Moreover, excessive deprotonation at higher pH values may generate negatively charged surface sites, potentially inducing electrostatic repulsion and further limiting adsorption.[31,32]

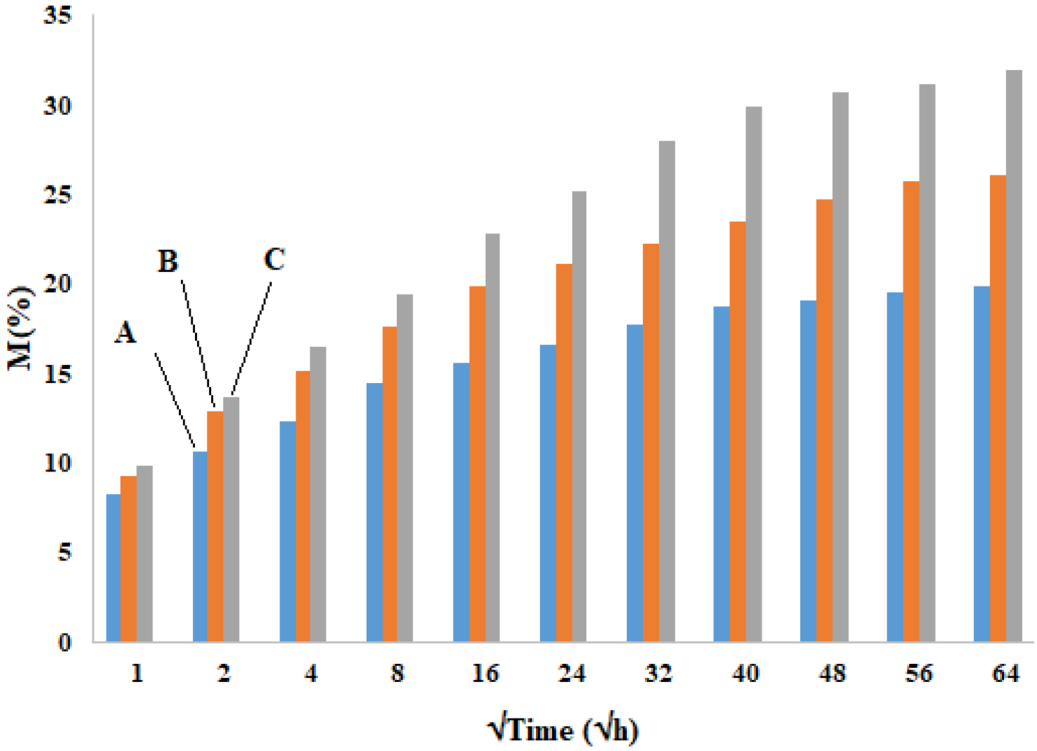

Fig. 3 Water adsorption potential of chitosan (A), chitosan-PEI (B), and chitosan-PEI-MTLPs polymeric systems (C).

The influence of adsorbent dosage on metal ion removal was evaluated using Chitosan-PEI-MTLPs quantities ranging from 0.3 to 1.5 g L^{-1} under fixed conditions (metal concentration: 800 mg L; pH: 6.5; solution volume: 50 mL, 45 °C) (Fig. 5). Increasing the dosage significantly enhanced adsorption efficiency, with Cd(II), Ni(II), and Pb(II) removal increasing from

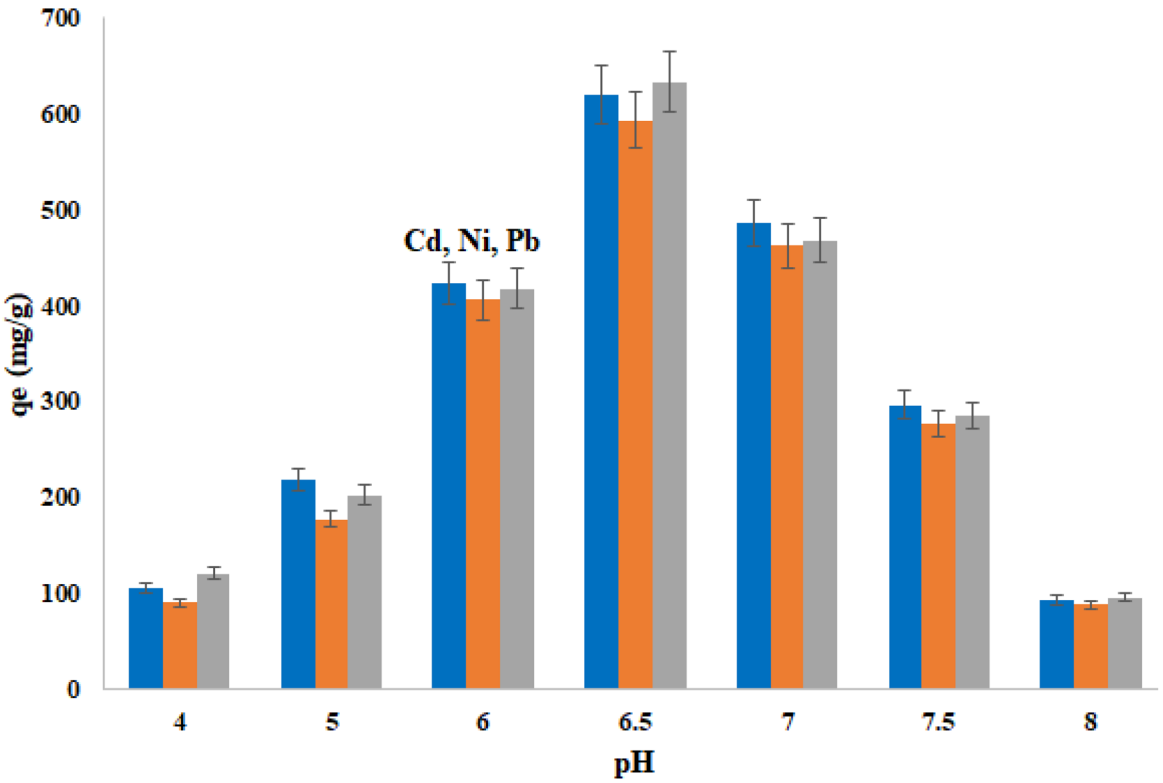

Fig. 4 Effect of pH (time: 120 min; adsorbent dosage: 1.2 g L^{-1}; Pb(II), Ni(II), and Cd(II): 800 mg L^{-1}; 45 °C).

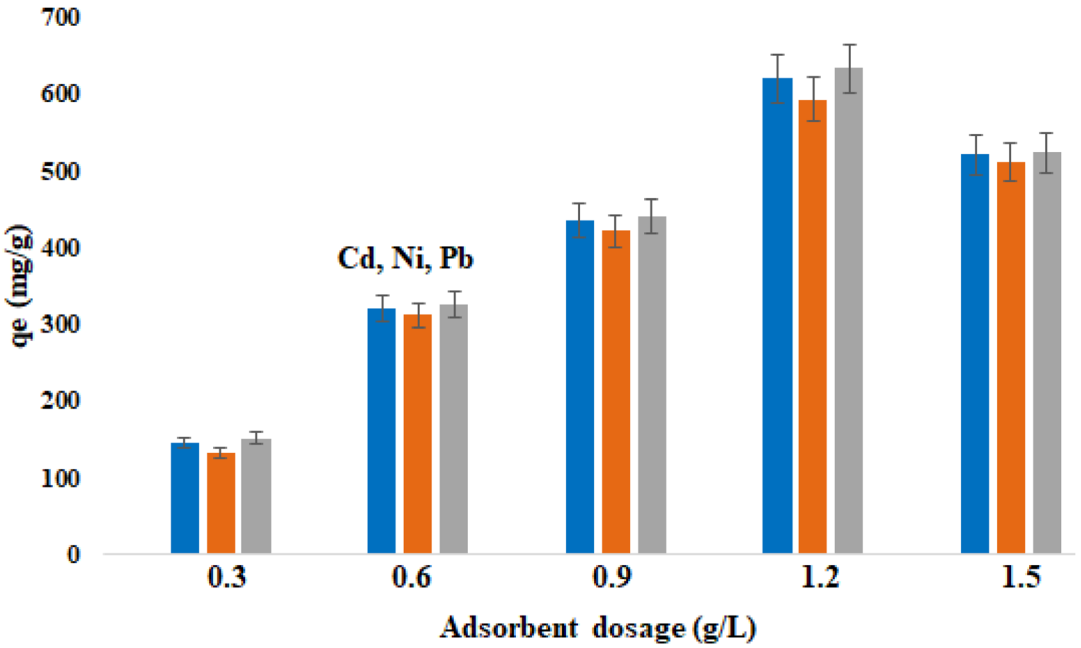

Fig. 5 Effect of adsorbent dosage (time: 120 min; pH: 6.5; Pb(II), Ni(II), and Cd(II): 800 mg L^{-1}; 45 °C).

145.6, 132.5, and 151.7 at 0.3 g L^{-1} to 620, 593.3, and 633.3 mg g^{-1} at 1.2 g L^{-1} respectively. Consequently, 1.2 g L^{-1} was identified as the optimal dosage for efficient adsorption performance.

As presented in Fig. 6, the adsorption capacity (q_e) of the Chitosan-PEI-MTLPs adsorbent increased proportionally with the initial metal ion concentration. At low concentrations (200 mg L^{-1}), removal efficiencies exceeded 95%, indicating a high availability of active sites and efficient metal–ligand interactions. As the concentration increased to 400–800 mg L^{-1}, q_e rose sharply and reached a maximum of 620 mg g^{-1} (Cd(II)), 593.3 mg g^{-1} (Ni(II)), and 633.3 mg g^{-1} (Pb(II)) at 800 mg L^{-1}. The increase in q_e reflects an enhanced driving force for mass transfer and more effective utilization of available binding sites. After that, at 1000 mg L^{-1}, due to the saturation of active sites, the adsorption capacities were not increased. Pb(II) consistently exhibited slightly higher q_e values compared to Cd(II) and Ni(II), which can be attributed to its stronger binding affinity and higher tendency to form stable complexes with the functional groups of the adsorbent.

Equilibrium adsorption data for Cd(II), Ni(II), and Pb(II) were analyzed using Langmuir, Freundlich, Temkin, and Dubinin–Radushkevich (D–R) models. Among them, the Langmuir isotherm exhibited the highest correlation coefficients (R^2 = 0.999), indicating monolayer adsorption on a homogeneous surface. The maximum adsorption capacities followed the order

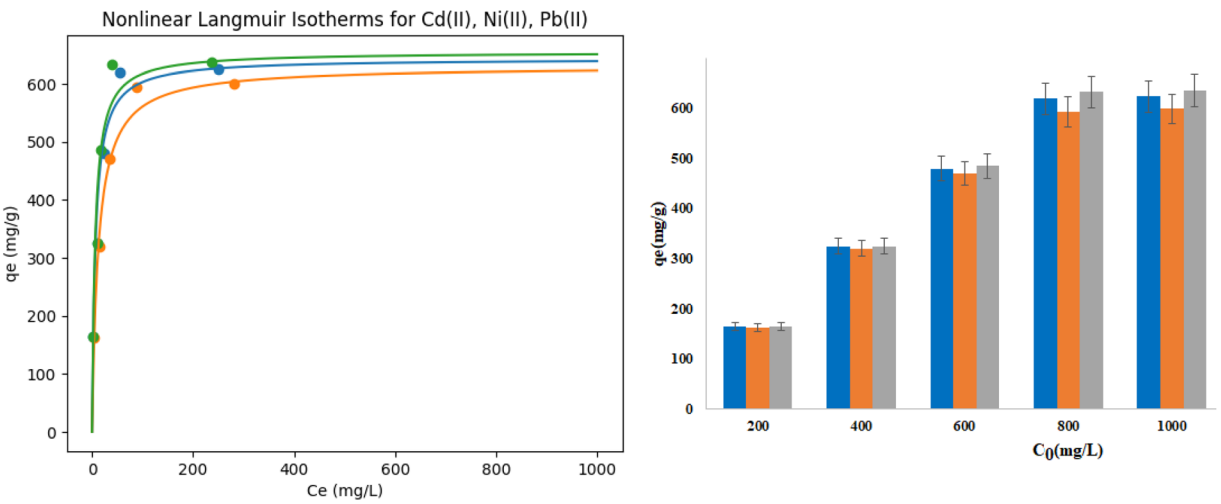

Fig. 6 Effect of initial Pb(II), Ni(II), and Cd(II) concentration (time: 120 min; adsorbent dosage: 1.2 g L^{-1}; pH: 6.5; 45 °C).

Table 2 Calculated parameters of isotherm models

Langmuir isotherm $\frac{1}{q_e} = \frac{1}{q_{max} K_l C_e} + \frac{1}{q_{max}}$	Cd(II) (q_{max}: 642.71; $K_l = 0.1509$; R^2: 0.9992)
	Ni(II) (q_{max}: 630.05; $K_l = 0.0807$; R^2: 0.9987)
	Pb(II) (q_{max}: 654.33; $K_l = 0.1646$; R^2: 0.999)
Freundlich isotherm $\log q_e = \log K_f + \frac{1}{n} \log C_e$	Cd(II) ($n = 3.47$; $K_f = 160.55$; R^2: 0.876)
	Ni(II) ($n = 3.04$; $K_f = 117.8$; R^2: 0.862)
	Pb(II) ($n = 3.41$; $K_f = 166.36$; R^2: 0.824)
Temkin isotherm $q_e = \frac{RT}{b} \ln (AC_e)$, $B = \frac{RT}{b}$	Cd(II) ($A = 3.04$; $B = 104.07$; R^2: 0.909)
	Ni(II) ($A = 1.08$; $B = 116.15$; R^2: 0.918)
	Pb(II) ($A = 3.25$; $B = 107.21$; R^2: 0.855)
Dubinin − Radushkevich(D − R) $\ln q_e = \ln q_{max} - K\varepsilon^2$, $\varepsilon = RT \ln \left(1 + \frac{1}{C_e}\right)$	Cd(II) (β: 1×10^{-6}; $E = 0.66$; R^2: 0.814)
	Ni(II) (β: 6×10^{-6}; $E = 0.30$; R^2: 0.861)
	Pb(II) (β: 1×10^{-6}; $E = 0.66$; R^2: 0.808)

Pb(II) > Cd(II) > Ni(II), with values of 654.3, 642.7, and 630.1 mg g^{-1}, respectively, demonstrating the strong affinity of the adsorbent toward heavy metal ions (Table 2, Fig. 6). Freundlich constants ($n > 3$) confirmed favorable adsorption, although lower R^2 values suggest limited surface heterogeneity. The Temkin model showed moderate agreement, implying a gradual decrease in adsorption energy with increasing surface coverage. The D–R model yielded mean adsorption energies below 1 kJ mol^{-1} for all metals, clearly indicating that physical adsorption dominates the uptake process, primarily driven by electrostatic interactions.

The time-dependent adsorption of Cd(II), Ni(II), and Pb(II) ions on the Chitosan-PEI-MTLPs surface is illustrated in Fig. 7. Rapid adsorption was observed during the first 60 min, with q_e

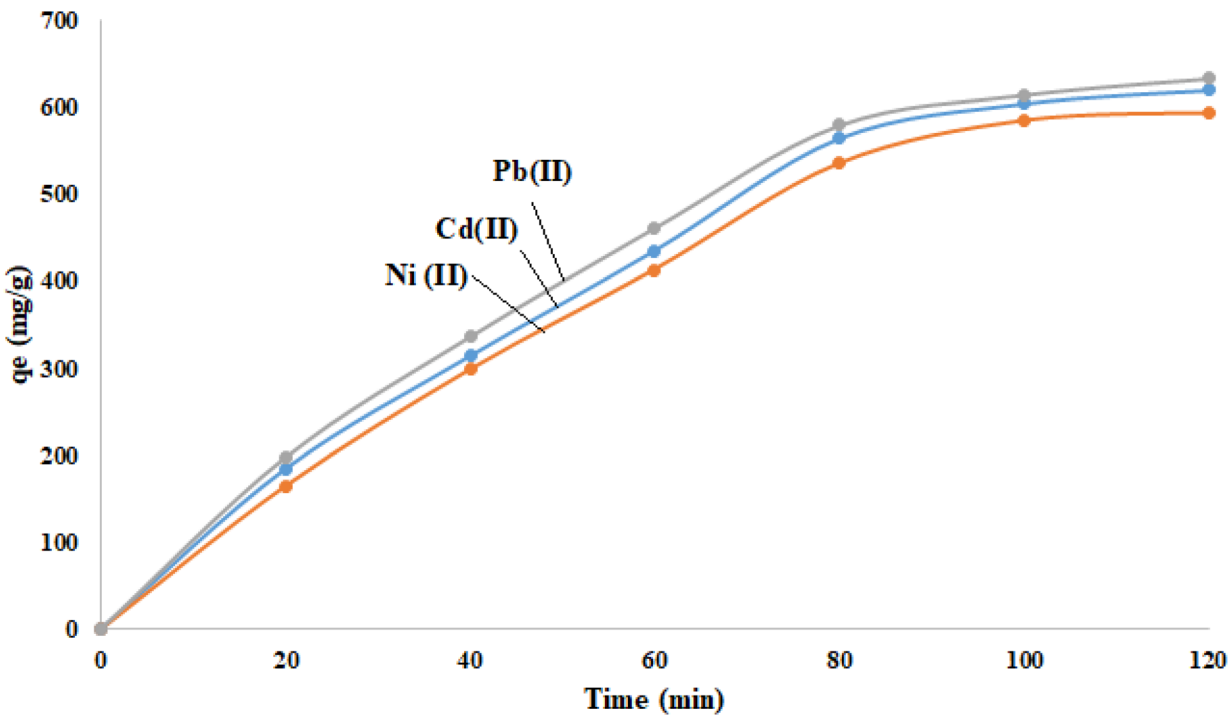

Fig. 7 Effect of contact time (pH: 6.5; adsorbent dosage: 1.2 g L^{-1}; Pb(II), Ni(II), and Cd(II): 800 mg L^{-1}; 45 °C).

Table 3 Calculated parameters of isotherm models

Model	Parameters (Cd(II))	Parameters (Ni(II))	Parameters (Pb(II))
Pseudo-first-order	K_1 (min^{-1}): 0.0419; R^2: 0.9361	K_1 (min^{-1}): 0.0471; R^2: 0.8977	K_1 (min^{-1}): 0.04; R^2: 0.9552
Pseudo-second-order	K_2 (g mg^{-1} min^{-1}): 7.0×10^{-6}; Q_e,calc (mg g^{-1}): 1284.47; R^2: 0.9426	K_2 (g mg^{-1} min^{-1}): 5.0×10^{-6}; Q_e,calc (mg g^{-1}): 1346.47; R^2: 0.9228	K_2 (g mg^{-1} min^{-1}): 8.0×10^{-6}; Q_e,calc (mg g^{-1}): 1204.84; R^2: 0.99604
Elovich	$\alpha = 0.0942$; $\beta = 0.00381$; $R^2 = 0.9770$	$\alpha = 0.0888$; $\beta = 0.00387$; $R^2 = 0.9798$	$\alpha = 0.1017$; $\beta = 0.00384$; $R^2 = 0.9823$
Intraparticle diffusion	K_{id} (mg g^{-1} $min^{-1/2}$): 72.11; $C = -128.20$; $R^2 = 0.9711$	K_{id} (mg g^{-1} $min^{-1/2}$): 70.94; $C = -141.04$; $R^2 = 0.9727$	K_{id} (mg g^{-1} $min^{-1/2}$): 71.32; $C = -105.35$; $R^2 = 0.9695$

values of 345.6 mg g^{-1} for Cd(II), 324.5 mg g^{-1} for Ni(II), and 365.6 mg g^{-1} for Pb(II). This initial phase corresponds to the availability of abundant active sites and strong electrostatic attraction between metal ions and surface functional groups. The adsorption rate subsequently decreased as sites became saturated, and equilibrium was attained after approximately 100–120 min, yielding equilibrium capacities of 620 mg g^{-1} (Cd(II)), 593.3 mg g^{-1} (Ni(II)), and 633.3 mg g^{-1} (Pb(II)).

The kinetic profiles for Cd(II), Ni(II), and Pb(II) reveal a rapid initial uptake followed by a gradual stabilization phase, indicating fast occupation of accessible surface sites and a slower transition toward equilibrium as diffusion resistance increases. Model fitting demonstrates that the pseudo-second-order and Elovich equations describe the experimental data more accurately than the pseudo-first-order model, implying that adsorption is mainly governed by surface chemical interactions rather than simple physical attachment (Table 3). The superior

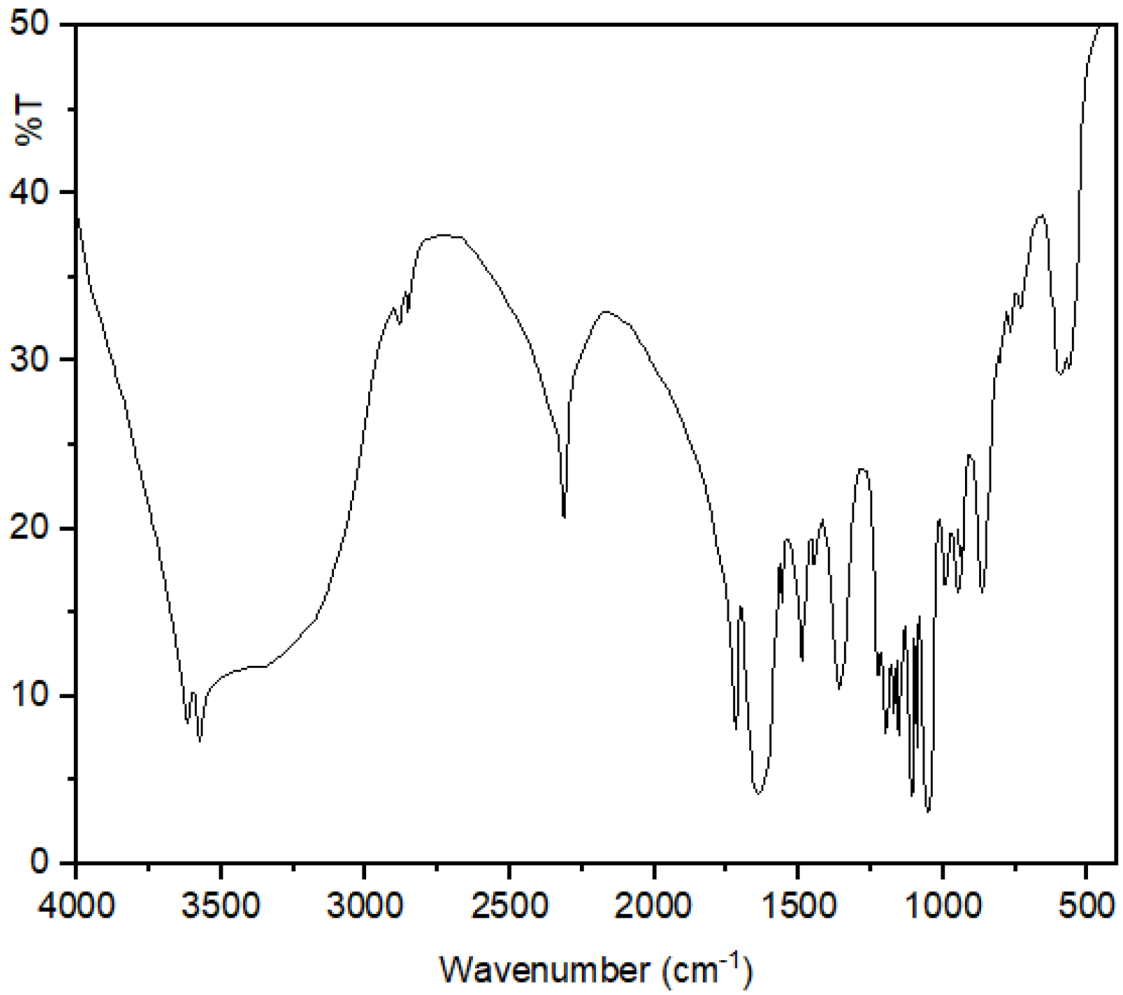

Fig. 8 FT-IR analysis of chitosan-PEI-MTLPs polymeric system after adsorption of Pb(II) ions.

performance of the Elovich model further reflects the heterogeneous nature of the adsorbent surface, where energetically diverse active sites participate in metal binding. This behavior suggests that complexation between divalent metal ions and functional groups on the catalyst surface plays a decisive role in controlling adsorption kinetics.

Although the intraparticle diffusion model shows high linearity, the nonzero intercept values confirm that diffusion within pores is not the sole rate-determining step and that boundary-layer effects significantly influence early-stage adsorption. Among the studied ions, Pb(II) exhibits the highest affinity toward the adsorbent, followed by Cd(II) and Ni(II), which can be attributed to differences in hydration strength and coordination tendencies that affect their ability to interact with surface ligands. Collectively, these findings indicate that adsorption proceeds through a multistep pathway dominated by chemisorption on heterogeneous active sites, supported by internal mass transfer, highlighting the strong potential of the synthesized catalyst for efficient heavy-metal sequestration in aqueous environments.

FT-IR analysis after the adsorption of Pb(II) ions reveals distinct modifications in its characteristic absorption bands, confirming the interaction between the polymer and the ions (Fig. 8). The broad and intense band typically observed at 3400–3450 cm^{-1} in pristine chitosan, attributed to overlapping O–H and N–H stretching vibrations and intermolecular hydrogen bonding, commonly shifts to lower wavenumbers and decreases in intensity after ion adsorption, indicating complexation through the lone pairs of oxygen and nitrogen atoms. In addition, the amide bands (C=O stretching, 1650–1700 cm^{-1}) exhibit shifts or reduced intensities, demonstrating the involvement of amine and carbonyl groups in metal binding. Changes in the C–N and C–O stretching vibrations (1000–1400 cm^{-1}) suggest alterations in the polymer backbone caused by coordination with metal ions.

Temperature exerted a significant influence on adsorption performance (Fig. 9). Increasing the temperature from 25 to 45 °C enhanced adsorption capacities. This trend indicates an endothermic process, wherein elevated temperature improves metal ion mobility, decreases solution viscosity, and accelerates diffusion to active sites. However, further increasing the temperature to 55–65 °C led to a gradual decline in adsorption capacity, likely due to partial desorption and weakening of adsorbate–adsorbent interactions. Pb(II) exhibited the highest adsorption at all temperatures, followed by Cd(II) and Ni(II), consistent with their respective ionic radii and hydration energies.

The thermodynamic parameters presented in Table 4 reveal that the adsorption of Cd(II), Ni(II), and Pb(II) onto the Chitosan-PEI-MTLPs polymeric system is temperature-dependent and endothermic in nature. The positive $\Delta G°$ values at 298 K

Table 4 Thermodynamic parameters of heavy metal adsorption process

	ΔG (kj mol^{-1})			ΔH (kj mol^{-1})	ΔS (j mol^{-1} K^{-1})
T (K)	Cd(II)	Ni(II)	Pb(II)	Cd(II): +65.14	Cd(II): +214
298	+1.75	+2.08	+1.61	Ni(II): +47.9	Ni(II): +158
308	−3.29	−2.97	−3.77	Pb(II): +72.8	Pb(II): +238
318	−6.36	−5.05	−7.30		
328	−4.30	−3.96	−4.49		
338	−3.02	−2.78	−3.21		

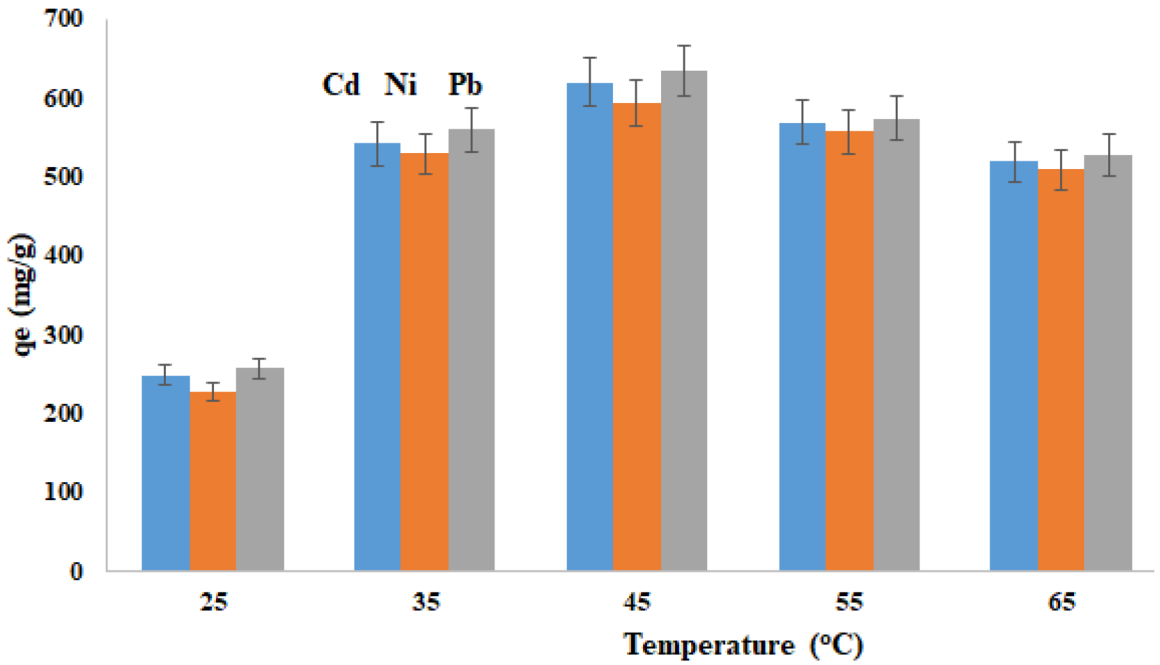

Fig. 9 Effect of temperature (pH: 6.5; adsorbent dosage: 1.2 g L^{-1}; Pb(II), Ni(II), and Cd(II): 800 mg L^{-1}).

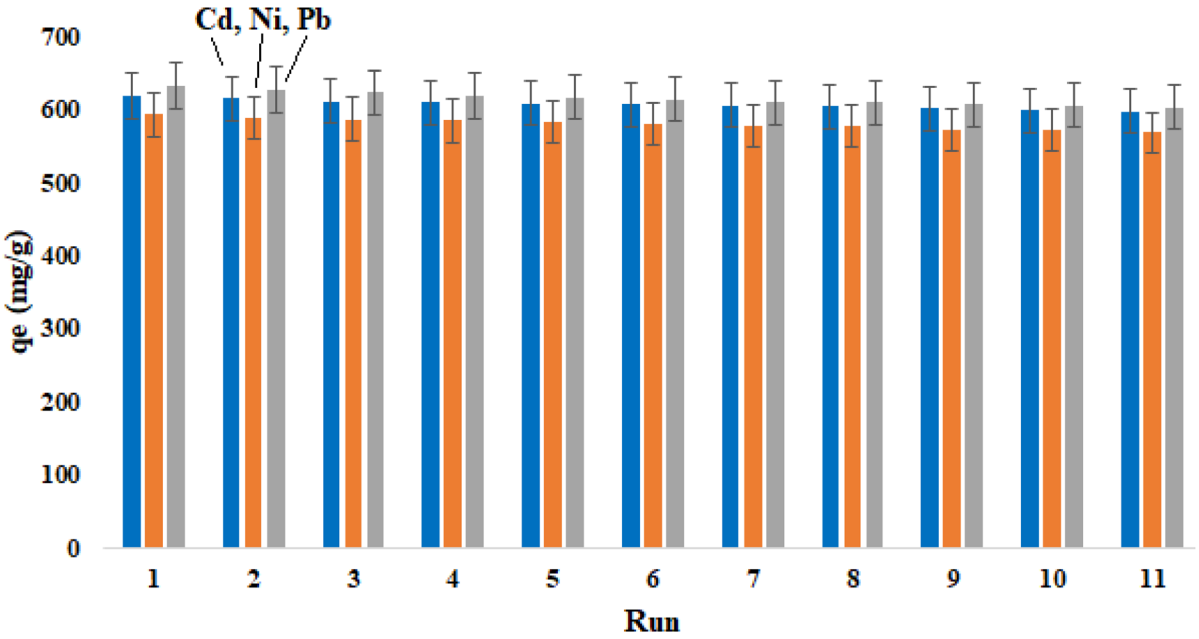

Fig. 10 Reusability of the Chitosan-PEI-MTLPs adsorbent over consecutive adsorption–desorption cycles.

indicate that the adsorption process is not favorable at lower temperature; however, the transition to negative ΔG° values at higher temperatures (308–338 K) confirms that adsorption becomes spontaneous with increasing temperature. The positive enthalpy values (ΔH° = +65.14 kJ mol^{-1} for Cd(II), +47.9 kJ mol^{-1} for Ni(II), and +72.8 kJ mol^{-1} for Pb(II)) demonstrate that heat absorption facilitates metal ion binding and suggest the involvement of strong interactions, likely coordination between metal ions and amino/hydroxyl functional groups of the polymer matrix rather than purely weak physical adsorption. Furthermore, the positive entropy changes (ΔS° = +214 J mol^{-1} K^{-1} for Cd(II), +158 J mol^{-1} K^{-1} for Ni(II), and +238 J mol^{-1} K^{-1} for Pb(II)) indicate increased randomness at the solid–solution interface, which can be attributed to desolvation of hydrated metal ions and structural rearrangement of polymer chains during complex formation.

The reusability of the Chitosan-PEI-MTLPs adsorbent was assessed over eleven successive adsorption–desorption cycles (Fig. 10). After five cycles, the capacities slightly decreased to approximately 94% of the original values, and after eleven cycles, the adsorbent retained 89–91% of its initial efficiency. The gradual decline is attributed to partial pore blockage, incomplete desorption, and minor degradation of active sites during regeneration. Pb(II) exhibited the highest retention, followed by Cd(II) and Ni(II). These findings confirm that the Chitosan-PEI-MTLPs material possesses excellent structural stability and regeneration potential, rendering it suitable for multiple reuse cycles in wastewater treatment applications.

4. Conclusion

This study successfully developed and characterized a biofunctionalized polymeric adsorbent, Chitosan-PEI-MTLPs, combining the amine-rich structure of chitosan and PEI with the high metal-binding affinity of naturally derived metallothionein-like proteins. The use of analytically pure reagents and precise synthesis conditions ensured high material purity, structural integrity, and reproducibility. Comprehensive characterization confirmed sequential modification and covalent immobilization of MTLPs, yielding a thermally stable and mechanically robust polymeric matrix. The Chitosan-PEI-MTLPs composite demonstrated remarkable adsorption capacities for Cd(II), Ni(II), and Pb(II) ions, exceeding 600 mg g^{-1}, governed primarily by monolayer physical adsorption on a homogeneous surface. Optimal adsorption occurred at near-neutral pH (6.5), with Pb(II) showing the strongest affinity due to its favorable ionic radius and hydration energy. Moreover, the adsorbent retained over 90% of its initial performance after multiple regeneration cycles, underscoring its structural durability and cost-effectiveness. Overall, the synthesized Chitosan-PEI-MTLPs polymer represents a new class of hybrid biopolymeric sorbents combining mechanical strength, biocompatibility, and high selectivity for heavy metals. Its high adsorption efficiency, reusability, and environmentally benign nature make it a promising candidate for sustainable wastewater treatment and environmental protection applications.

Author contributions

N. Sheykhan, and A. Szuławska-Mroczek, performed the experiments and analyzed the data. M. Ghashang is the corresponding author, having prepared the materials and written the paper.

Conflicts of interest

The authors declare that they have no interest to influence the work reported in this paper.

Data availability

The data that could support our findings is available in the text of this article.

Acknowledgements

The laboratory support by the Islamic Azad University, Najafabad Branch is highly acknowledged.

References

1 K. Jomova, S. Y. Alomar, E. Nepovimova, K. Kuca and M. Valko, Heavy metals: Toxicity and human health effects, *Arch. Toxicol.*, 2025, **99**, 153–209.
2 M. Balali-Mood, K. Naseri, Z. Tahergorabi, M. R. Khazdair and M. Sadeghi, Toxic mechanisms of five heavy metals: Mercury, Lead, Chromium, Cadmium, and Arsenic, *Front. Pharmacol*, 2021, **12**, 643972.
3 S. R. Dhokpande, S. M. Deshmukh, A. Khandekar and A. Sankhe, A review outlook on methods for removal of heavy metal ions from wastewater, *Sep. Purif. Technol.*, 2024, **350**, 127868.
4 S. Sheikh, O. Naghizadeh-Dehno, S. Mirkhalafi and M. Ghashang, Magnetic heterogenization of supramolecular carbohydrates for the efficient adsorption of heavy metals removal from wastewater, *Inorg. Chem. Commun.*, 2024, **168**, 112835.
5 F. Aminsharei, A. Lahijanian, A. Shiehbeigi, S. Shieh Beiki and M. Ghashang, Dual magnetization and amination of cellulosic chains for the efficient adsorption of heavy metals, *Int. J. Biol. Macromol.*, 2024, **276**, 134004.
6 P. Torkian, S. M. Mortazavi Najafabadi, D. Grzelczyk and M. Ghashang, TiO2 bonded SiO_2-alkyl-NH_2 grafted cellulose for improving thermal stability, mechanical strength characteristics, and water adsorption capacity, *Cellulose*, 2024, **31**, 1801–1812.
7 M. Khalaj and M. Ghashang, An investigation of the mechanical properties and adsorption potentials of Fe_2O_3@SiO_2-L-cysteine-cellulose system, *Sci. Rep.*, 2025, **15**, 8413.
8 Y. Mei, S. Zhuang and J. Wang, Adsorption of heavy metals by biochar in aqueous solution: A review, *Sci. Total Environ.*, 2025, **968**, 178898.
9 C. Y. Hsu, Y. Ajaj, Z. H. Mahmoud, G. K. Ghadir, Z. K. Alani, M. M. Hussein, S. A. Hussein, M. M. Karim, A. Al-khalidi, J. K. Abbas, A. H. Kareem and E. Kianfar, Adsorption of heavy metal ions use chitosan/graphene nanocomposites: A review study, *Results Chem.*, 2024, **7**, 101332.
10 Y. G. Ko, Hybrid method integrating adsorption and chemical precipitation of heavy metal ions on polymeric fiber surfaces for highly efficient water purification, *Chemosphere*, 2024, **363**, 142909.
11 P. Rostami, M. R. Moradi, M. A. Pordsari and A. Ghaemi, Carboxylic acid functionalized para-xylene based hypercrosslinked polymer as a novel and high-performance adsorbent for heavy metal removal, *Arab. J. Chem.*, 2024, **17**, 105634.
12 M. Priyadarshanee and S. Das, Spectra metrology for interaction of heavy metals with extracellular polymeric substances (EPS) of Pseudomonas aeruginosa OMCS-1 reveals static quenching and complexation dynamics of EPS with heavy metals, *J. Hazard. Mater.*, 2024, **466**, 133617.
13 J. Bayar, N. Ali, Y. Dong, U. Ahmad, M. M. Anjum, G. R. Khan, M. Zaib, A. Jalal, R. Ali and L. Ali, Biochar-based adsorption for heavy metal removal in water: A sustainable and cost-effective approach, *Environ. Geochem. Health*, 2024, **46**, 428.
14 V. R. Kondakindi, R. Pabbati, P. Erukulla, N. R. Maddela and R. Prasad, Bioremediation of heavy metals-contaminated sites by microbial extracellular polymeric substances – A critical view, *Environ. Chem. Ecotoxicol.*, 2024, **6**, 408–421.
15 X. Jiang, J. Guo, M. Sun, Q. Sun, W. Ding, H. Li and H. Zheng, Simultaneous adsorption of Ciprofloxacin and Ni(II) from wastewater using poly(vinyl alcohol)/poly(sodium-p-styrene-sulfonate) semi-interpenetrating polymer network@Ni foam: Insights into the synergistic and antagonistic mechanisms, *Chem. Eng. J.*, 2024, **486**, 150391.
16 A. Iqbal, E. Cevik, A. Mustafa, T. F. Qahtan, M. Zeeshan and A. Bozkurt, Emerging developments in polymeric nanocomposite membrane-based filtration for water purification: A concise overview of toxic metal removal, *Chem. Eng. J.*, 2024, **481**, 148760.
17 C. Shi, R.-G. Zeng, S.-C. Yuan, L. Zhang, X.-Y. Wang, L.-T. Hao, X.-D. Hao, N. Zhang and Y.-Y. Wu, Preparing a heavy-metal adsorbent based on alginate-like extracellular polymers from conventional activated sludge via polyethyleneimine grafting, *Sustain. Chem. Pharm.*, 2024, **38**, 101472.
18 Y. Zou, Cu^{2+}, Cd^{2+}, and Pb^{2+} ions adsorption from wastewater using polysaccharide hydrogels made of oxidized carboxymethyl cellulose and chitosan grafted with catechol groups, *Iran. Polym. J.*, 2024, **33**, 57–66.
19 A. Mondal, M. Haque, A. Aggarwal, M. Kalita and A. Singha Roy, Protein-based hydrogel for environmental remediation: Removal of hazardous metal ions and toxic organic dyes from wastewater, *J. Mol. Liq.*, 2025, **423**, 127174.
20 S. Bandehali, A. Moghadassi, S. M. Hosseini, F. Parvizian, D. Ghanbari, R. Rahimizadeh and A. Afshar Ebrahimi, Smart ion exchange membrane with high impact in heavy metals separation prepared by electrospinning process with ultrasensitive responsiveness for water treatment, *Chem. Eng. Res. Des.*, 2024, **205**, 763–774.
21 J. Wang, M. Zhu and J. Zhou, Preparation of a porous protein-based composite material by in situ polymerization of Pickering high internal phase emulsion for adsorption of lead ions, *ACS Omega*, 2024, **9**, 20142–20151.
22 W. Bie, S. Zhang, L. Zhang, H. Li, X. Sun, T. Cai, Z. Wang, F. Kong and W. Wang, Thioether-functionalized porous β-cyclodextrin polymer for efficient removal of heavy metal ions and organic micropollutants from water, *Carbohydr. Polym.*, 2024, **324**, 121509.
23 S. Hu, T. Huang, N. Zhang, Y. Lei and Y. Wang, Chitosan-assisted MOFs dispersion via covalent bonding interaction

toward highly efficient removal of heavy metal ions from wastewater, *Carbohydr. Polym.*, 2022, **277**, 118809.
24 L. Boughrara, F. Z. Sebba, H. Sebti, E. Choukchou-Braham, B. Bounaceur, S. Ould Kada and F. Zaoui, Removal of Zn(II) and Ni(II) heavy metal ions by new alginic acid-ester derivatives materials, *Carbohydr. Polym.*, 2021, **272**, 118439.
25 U. Upadhyay, I. Sreedhar, S. A. Singh, C. M. Patel and K. L. Anitha, Recent advances in heavy metal removal by chitosan-based adsorbents, *Carbohydr. Polym.*, 2021, **251**, 117000.
26 Y. Niu, W. Hu, M. Guo, Y. Wang, J. Jia and Z. Hu, Preparation of cotton-based fibrous adsorbents for the removal of heavy metal ions, *Carbohydr. Polym.*, 2019, **225**, 115218.
27 R. Yang, D. Roshani, B. Gao, P. Li and N. Shang, Metallothionein: A comprehensive review of its classification, structure, biological functions, and applications, *Antioxidants*, 2024, **13**, 825.
28 N. Zaręba and M. Kepinska, The function of transthyretin complexes with metallothionein in Alzheimer's disease, *Int. J. Mol. Sci.*, 2020, **21**, 9003.
29 T. V. Divya, P. Chandwadkar and C. Acharya, NmtA, a novel metallothionein of Anabaena sp. strain PCC 7120 imparts protection against cadmium stress but not oxidative stress, *Aquat. Toxicol.*, 2018, **199**, 152–161.
30 Y. Yu, K. Shi, X. Li, X. Luo, M. Wang, L. Li, G. Wang and M. Li, Reducing cadmium in rice using metallothionein surface-engineered bacteria WH16-1-MT, *Environ. Res.*, 2022, **203**, 111801.
31 F. Fu and Q. Wang, Removal of heavy metal ions from wastewaters: A review, *J. Environ. Manage.*, 2011, **92**, 407–418.
32 J. Wang and C. Chen, Biosorbents for heavy metals removal and their future, *Biotechnol. Adv.*, 2009, **27**, 195–226.